Experimental and numerical true strain assessment on sheet forming for different tool design

Ravilson Antonio Chemin Filho & Heber Castro Silva &
Paulo Victor Prestes Marcondes

Received: 30 March 2009 / Accepted: 2 September 2009

Abstract The forming tests are being developed with the purpose of enabling forming companies to better understand the sheets formability. The identification of the regions where tension-tension, tension-compression, and/or plane strain occurred during the forming process can aid the process planning through the tools geometry optimization. This work consisted of evaluating, experimental and numerically, the major true strain obtained with different punch designs, which were used in addition to the traditional Nakazima test tool. The main objective was to study the true strain profile as an alternative method to analyze the tool design influence on stretching forming of high stampability steels (DC 06). The friction coefficient was investigated, and an evaluation was also made of the chosen program's response quality (validation). The results are given as a major true strain distribution profile at points distributed linearly from the region close to the die radius to the punch pole. The result expectation is to help the process planning and the material evaluation based on the correct tool design specification in order to obtain the desired true strain distribution in the formed part.

Keywords Forming . Tool design . Modeling

R. A. Chemin Filho : H. C. Silva : P. V. P. Marcondes
Universidade Federal do Paraná/DEMEC,
Av. Cel. Francisco H. dos Santos, 210,
CEP 81531-990 Curitiba, Paraná, Brazil
e-mail: marcondes@ufpr.br
R. A. Chemin Filho
e-mail: ravilson@pop.com.br
H. C. Silva
e-mail: hebercs@uol.com.br

1 Introduction

Steel sheets have become the most important raw material for the manufacture of large variety of stamped durable consumer goods.

Stamping dies are traditionally designed by professionals with practical experience who can determine the best stamping process configuration for each shape based on the use of tryout techniques, the circle grid analysis method, and the Forming Limit Curve [1].

According to Makinouchi [2], changes are often necessary when trying out stamping tools. Such changes may range from the choice of a new material with better formability to adjustments in the dies and punches design in order to achieve the degree of satisfaction expected for the product [3,4]. All these actions, however, require time and money creating the need for better true strain distribution profile knowledge during processing. The identification of regions of tension-tension, tension-compression, and/or plane strain during forming can contribute to improve the stamping process through tools geometry optimization [5,6]. The major and minor true strains can be determined with precision, leading to identification of each deformation zone and eventually to methods for preventing stamping defects [7].

Since there exists rarely an analytical expression describing the relationships between these designs parameters, the dimensioning and integration of the tooling elements constituting the forming interface follow a series of costly try-and-error procedures on the workshop floor [8]. Formability analysis of the sheet materials is usually evaluated through the concept of Forming Limit Diagrams. Some analytical models are being developed but the construction of Forming Curves for particular materials is still basically experimental.

Predicting sheet behavior through numerical simulation is an important design tool, since it allows reducing the number of practical tests to be carried out prior to the tool's completion and delivery to the client. Simulation also allows one to predict the critical strain areas in workpieces allowing modifications to be made in the dies, or even in the product, while still in the design phase. Moreover, analytical or experimental solutions that can easily describe all the possible strains pathways for this type of operation are almost impossible [9].

This paper analyzes the major true strain distribution profile produced along the stamped sheet metal using different punch geometries in order to identify the sheet deformation uniformity during the forming operation. A numerical analysis is also made, and the results expectation is to help the process planning and the material evaluation in order to obtain the desired strain distribution in the formed part reducing the costly try-and-error procedures. As we analyzed a simple shape part, the Forming Limit Strain technique was chosen instead the Forming Limit Stress approach—independently on strain path [10].

2 Experimental methodology

The material used was a cold-rolled mild steel alloy produced by Thyssen Krupp to the DC06 specification (0.7 mm thickness). In this study, thin square 200 mm-sided sheets were used as test specimens and stretched using different punch geometries (Fig. 1).

An important factor in the development of the geometry of each punch was the specification of the R1 and R2 radii, the former corresponding to the punch head size (diameter) and the latter responsible for the congruence of R1 with the rectilinear portion of the tool. The congruence between these radii was the determining factor in assigning the aforementioned shapes to each punch. The position of the major true strain peak (ε_1) allows identifying which part of the punch acted in this region, i.e., whether the material's maximum ε_1 was caused by the punch head radius (R1) or by the external congruence radius (R2).

A 4.2-mm diameter circles grid was imprinted on the test specimen's surface. The grid was imprinted using a new process developed during this research, which differs from the processes traditionally used (electrolytic, photosensitive resin, or laser marking). This new marking process uses a screen (mask) similar to the kind used in the silkscreen technique, and a grid fixer developed for the coated metallic sheet employed (mixture of 25% of nitric acid, solvent, and black metallic paint). The process proved simpler, easier to apply, and cheaper, since no special equipment is required to the grid imprint.

Figure 2 shows the analyzed path, and the measurements were taken on the opposite side of the fracture so that the measurements in cracked circles were avoided. The printed circles were measured with a calibrated transparent mylar tape with diverging railroad tracks. An average of three test specimens was evaluated for each one of the punch geometries.

In order to evaluate the ability of the ANSYS 9.0/LS_Dyna software to reproduce the experiments, some numerical tests were carried out following the methodology described below.

Preprocessing This phase consisted of analyzing the input data required in the preprocessing phase, such as the tools' geometries, material characteristics [11], element type formulation, constraints, and loadings. Due to the symmetry of the problem, only one quarter of the geometry of each component was built.

The punch downward velocity used for the simulations was 400 mm/s. The velocity used for the experiments was 1.33 mm/s, but higher velocities than the real ones can be used in explicit dynamic analyses [12]. The necessary condition to use higher velocities is that the kinetic energy remains below a certain level so that the dynamic effect does not affect the simulation [13].

The punch, die, and blank holder were defined as rigid bodies. Considering the plane formed by x- and z-axes, a plane parallel to the sheet, the following constraints were applied to the rigid bodies, conditions 1, 2, and 3 (Fig. 3). For the punch and blank holder, the movement in the x- and z-axes is equal to zero, and the rotation about the x-, y-, and z-axes is equal to zero. For the die, the movement in the x-, y-, and z-axes is equal to zero, and the rotation about the x-, y-, and z-axes is equal to zero.

The Shell163 type element was used to model the sheet and the Solid164/rigid type was used to model the punch, die, and blank holder [14]. The following formulation were used for the shell elements: S/R Hughes-Liu type formulation, number of integration points in the thickness direction equal to five, integration rule of Gauss quadrature, and nodal distance of 2.5 mm (when local refinement of the grid was not indicated) and 0.8 mm (when local refinement was indicated). The material tested experimentally was characterized as anisotropic, and the Barlat's model was selected [15]. The material properties are listed in Table 1.

To formulate the contact condition between the solid bodies and the sheet it was formed components with the nodes of each elements and imposed the automatic contact condition between the main and slave surfaces, so that the nodes with potential contact were searched automatically by the program.

Processing In this phase, the model was simulated using LS_Dyna software. Initially, the forming operation with the hemispherical punch (P3) was simulated, and different friction coefficient values were tested. The value providing the best curve fit (validation) in relation to the experimental data was used in the all other simulations. The numeric error can be defined as the difference between the exact analytical solution of a certain variable of interest and its numeric solution [16]. The main processes to estimate and to evaluate the error in simulation programs are called verification and validation. While the verification is the evaluation of the computational solution accuracy in relation to the numeric model, the validation seeks to determine the proximity that the mathematical model is from the real phenomenon, through the comparison of the numeric solution with the experimental data [17]. Always, it was used mapped (structured) meshing with quad-type elements.

3 Results and discussion

Figure 4 illustrates the true strain distribution profile of test specimen stamped with different punch geometries. Figure 4a shows a ε_1 peak between points 3 and 4 in the exact position of the tool's external congruence radius (R2). This punch geometry (P1) does not present any curvature at the punch head, which is flat, so that the highest stress level and hence, the ε_1 (in the range of 0.14) are limited to this region of the tool.

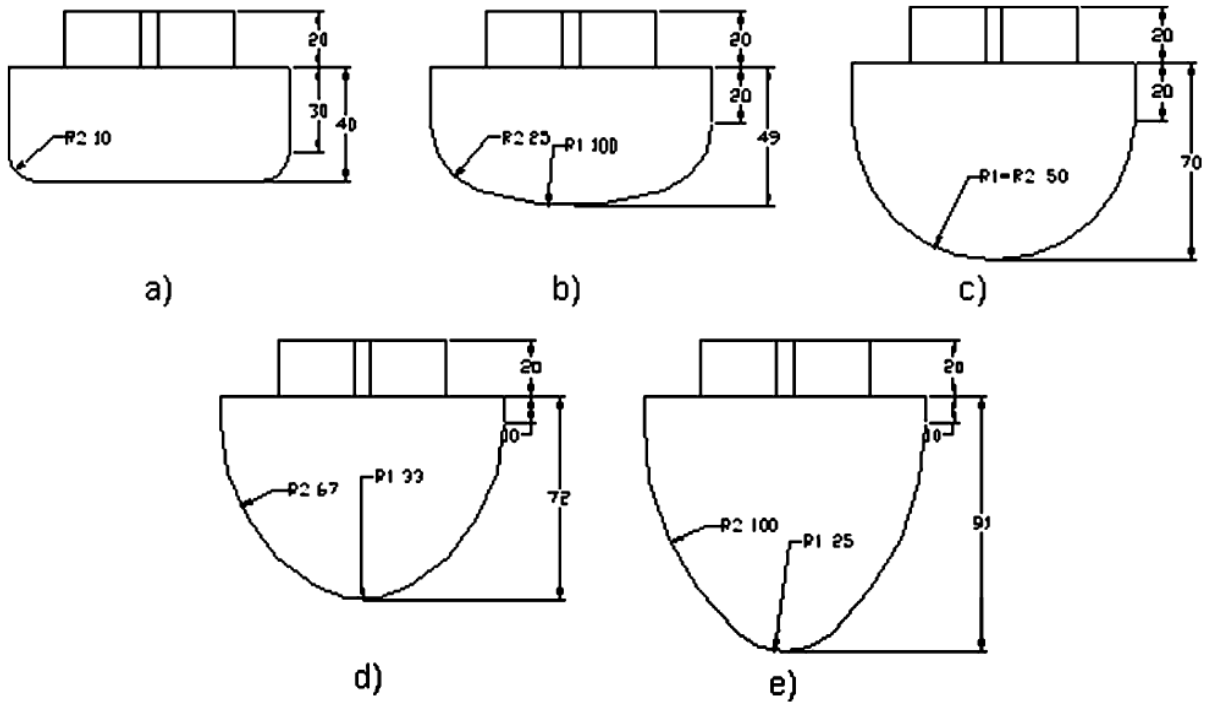

Fig. 1 Geometry of the punches and congruence radii of each tool—100 mm diameter. a Cylindrical punch (P1). b Shallow ellipse punch (P2). c Hemispherical punch (P3). d Deep ellipse punch (P4). e Extra deep ellipse punch (P5)

A comparison of the curve obtained in the test with the cylindrical punch (P1) with the curve obtained with the shallow ellipse-shaped punch (P2; Fig. 4a, b) indicates that the ε_1 peak shifted to a slightly higher degree (0.15), while its position was concentrated at points 4 and 5 (shifting visibly away from the die radius toward the punch pole). The ε_1 location and displacement of this peak to the right (toward the punch pole) are due to the increase of the external radius (R2) and the existence of an R1 radius at the head of punch P2. This geometrical characteristic of the tool kept the ε_1 peak at the external radius (R2) because in this case the congruence radius is much smaller than the punch head radius (R1). The slight increase in the ε_1 peak from 0.14 for punch P1 to 0.15 for punch P2 occurred because the external radius R2 (punch P2) was larger than the external radius of punch P1, which generated a lower stress concentration in this critical region (allowing the sheet to reach a slightly higher stampability).

Figure 4c depicts the major true strain distribution profile for the hemispherical punch (P3), which corresponds to the model originally used in Nakazima tests. The ε_1 distribution profile obtained with punch P3 showed the same tendency as the curve resulting from the ε_1 measurements of punch P2 with the major true strain peak displaced to the punch pole direction (right-hand side of the graph). The punch P3 caused this variation in the curve to increase further, with the ε_1 peak in the range of 0.29 (ε_1 peak was positioned between points 6 and 7).

Both the increase in true strains and the shift of the curve's peak toward the punch pole were greater than the variation presented by punch P2 when compared with punch P1. An analysis of these results based on the tool's geometry indicates that the hemispherical punch presented a single radius that encompassed the entire punch profile. In other words, there was no congruence between an external radius (R2) and an internal one (R1) that could concentrate stresses in a specific position of the material under the tool influence. Therefore, the uniform geometry of punch P3

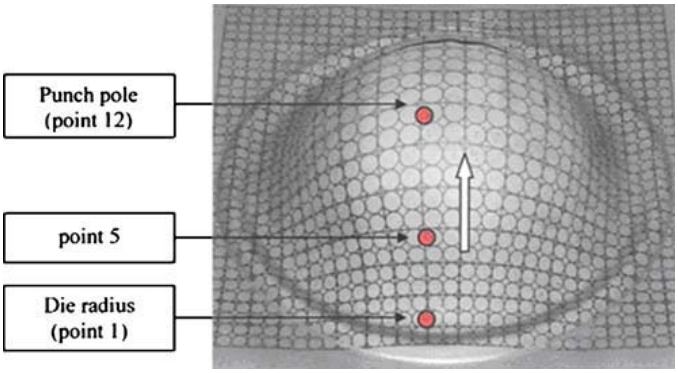

Fig. 2 Test specimen showing the measured points for the true strain distribution profile

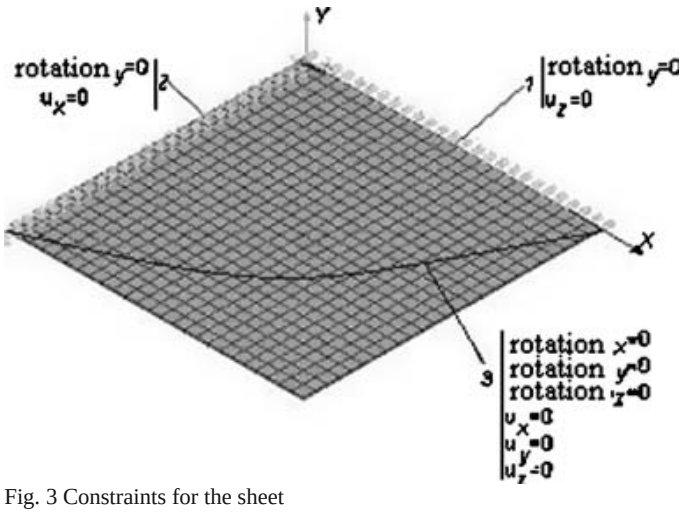

Fig. 3 Constraints for the sheet

Table 1 DC 06 main properties

Property	Value	Unit	Source
Density (ρ)	7.850	g/cm^3	Literature
Modulus of elasticity (E)	210,000	MPa	Literature
Poisson's coefficient (ν)	0.3	(Dimensionless)	Literature
Plastic resistance constant (K)	626.8	MPa	Tension test
m	6	(Dimensionless)	Literature
Anisotropy coefficient at 0° (R_0)	2.0483	(Dimensionless)	Tension test
Anisotropy coefficient at 45° (R_{45})	1.8659	(Dimensionless)	Tension test
Anisotropy coefficient at 90° (R_{90})	2.5988	(Dimensionless)	Tension test

generated a better stress distribution on the material surface, allowing the sheet to reach a higher formability at an intermediary point between the die radius and the punch pole (corresponding to the tool's curvature radius, i.e., being the main point of action of the punch on the sheet).

Altering the punch configuration to geometry with a sharper punch head radius (R1) and a larger external congruence radius (R2) motivated the ε_1 peak to shift even further toward the punch pole. This variation in the major true strain distribution is shown in Fig. 4d, e, which illustrate the results on test specimens with the deep ellipse (P4) and extra deep ellipse (P5) punches, respectively. Both tools had a smaller R1 radius at the punch head that tended to favor a higher stress concentration in this region (which explains the displacement of the major true strain peaks to the punch pole position).

From the curves obtained for punches P4 and P5, it is clear that the ε_1 peak was positioned at point 8 for P4 and at point 9 for P5 (which had an even smaller R1 radius than P4) while, for the hemispherical punch (P3), this extreme point was situated between points 6 and 7. These data indicates that the reduction of the radius at the punch pole caused the tool to act preferentially in the central portion of the tested sample, making this the sheet region of maximum ε_1. The surrounding region of the material was not in direct contact with the stamping punch, so it did not undergo true strain as severe as that in the sheet metal central area.

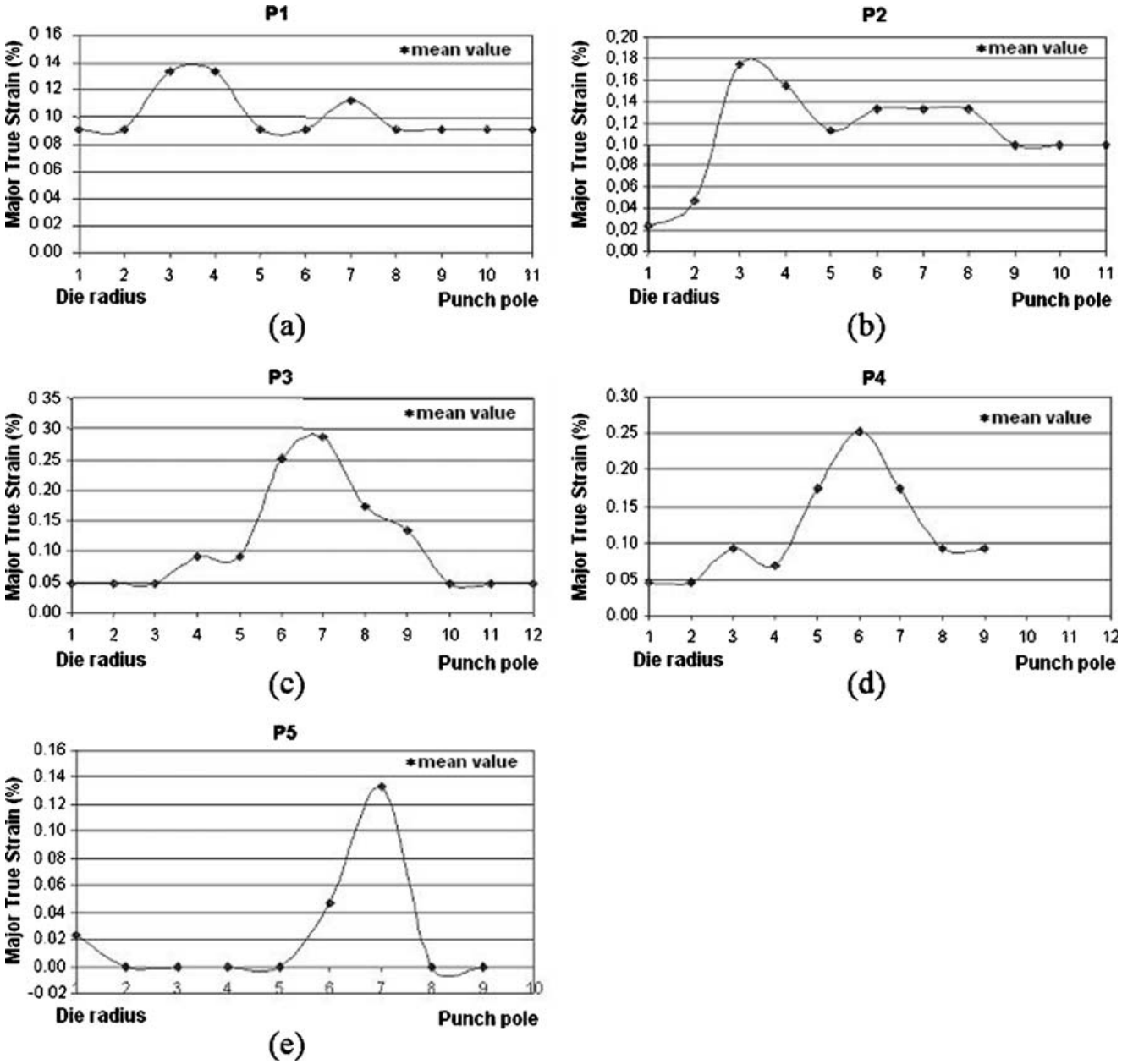

Fig. 4 True strain distribution profile of the 200×200 mm test specimen (experimental): a) cylindrical punch (P1), b) shallow-ellipse punch (P2), c) hemispherical punch (P3), d) deep-ellipse punch (P4) and e) extra deep-ellipse punch (P5)

The smaller the punch head radius, the greater is the material stress concentration leading to a lower stampability degree. This statement is reinforced by the results obtained for the maximum ε_1 degrees illustrated in the curves shown in Fig. 4d, e. Since P4 showed a smaller R1 radius than P3, it is clear that the curve resulting from the tests with this punch had its point of maximum ε_1 reduced to 0.24, while punch P5 (whose radius is even smaller than P4) promoted an even smaller ε_1 peak of around 0.13.

In a sequence from punches P1 to P5, the characteristics of the aforementioned curves clearly indicate that, the more uniform the tool geometry the more homogeneous the stress distribution in the stamped material (enabling the material to reach higher true strain degrees).

In order to validate the numerical data for the different punch geometries, the major true strain curves (ε_1) obtained experimentally and by simulation were plotted.

Figure 5 illustrates the ε_1 distribution profile with the hemispherical punch (P3) as a function of the distance from the punch pole for different friction coefficients, i.e., between 0.0 and 0.20. The experimental values without lubricant addition are also presented.

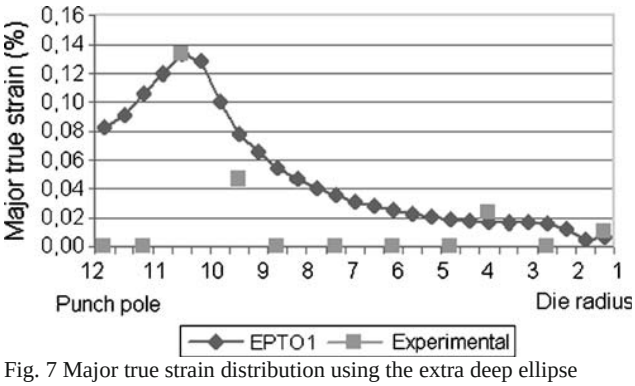

Fig. 7 Major true strain distribution using the extra deep ellipse punch (P5)

In the zero friction condition, the strain distribution reached a maximum value close to the punch pole (point 12

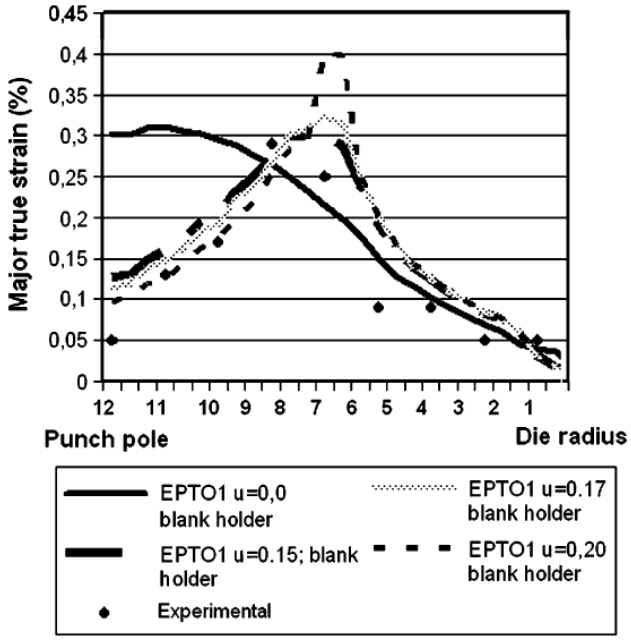

Fig. 5 The major true strain distribution as a function of distance from the center of the hemispherical punch (P3) and the friction coefficient

of Fig. 2) decreasing as it got further away from that region. With a friction coefficient other than zero, the contact with the punch restrains the sheet movement. Thus, the value of ε_1 decreased at the punch center region as the friction coefficient increased. Because the ε_1 distribution in the contact region with the die is also restricted (both by the blank holder and by the friction with the die), the region of maximum ε_1 is now the region not in contact either with the punch or the die. Figure 5 also shows that the simulated values for a friction coefficient of 0.15 are in good agreement with the experimental ε_1 peak values in the region between the die and the punch radii. In the region corresponding to the punch pole, the experimental ε_1 values were slightly lower than those found for this friction value. In the sheet center, the ε_1 values are about 0.15, gradually increasing up to 0.35 in the region between the punch pole and the die radius. From this region, the ε_1 value diminishes up to the region of contact with the die.

Figure 6 shows the ε_1 distribution with the cylindrical punch (P1) in the direction from the die radius to the punch pole. The grid was refined in the region corresponding to the ε_1 peak.

Note that at the end of curves, i.e., at the points corresponding to the die radius and the punch pole, the simulation results are just below the experimental data (using the refined grid). On the other hand, the unrefined grid showed a good agreement with the experimental results in the region of the punch radius (maximum ε_1) and in the region between the punch and the die radii. We also can observe that the grid with local refinement was able to reflect an experimental inflection point, as indicated in Fig. 6, which was not the case with the locally unrefined grid. Similarly, the ε_1 was quite low in most of the punch contact area. This was due to the action of the punch in a large region of the sheet imposing a greater strain restriction.

The extra deep ellipse punch (P5) was simulated using the same parameters as those employed to simulate the hemispherical punch (P3), i.e., a grid without local refinement and a 0.15 friction coefficient. Figure 7 compares the ε_1 obtained by experimental and numerical analysis. The simulation data presented a good agreement to the experimental results, with the ε_1 peak coinciding in magnitude and location, as well as the shape of the curve.

The experimental results showed values of zero for the ε_1 in the region corresponding to the punch pole and after the maximum ε_1 region. On the other hand, the simulated values started at 0.08 (punch pole) gradually declining to 0.02 in the region between the highest value and the die radius. A possible explanation for this difference is that the experimental data reading method is limited by the system resolution used (which was probably not able to detect oscillations in the deformation values around 0.02).

Fig. 6 The true strain distribution comparison and the experimental data for the cylindrical punch (P1)

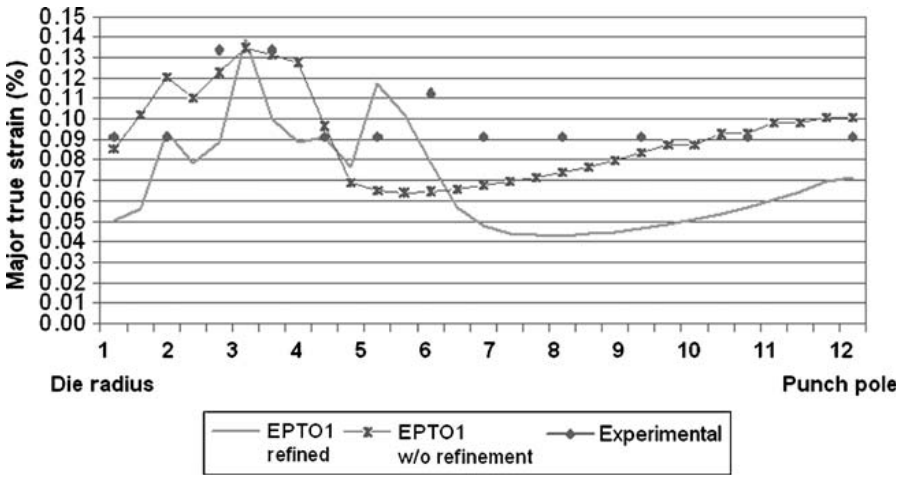

We can observe the ε_1 values are concentrated in the punch contact region and decline to values close to zero along a few millimeters causing a high major true strain gradient. The highest ε_1 value was also located in the sheet's central region, which corresponds to the punch contact region. In the contact region with the die radius, the major true strains values were negative and close to zero. Thus, the sheet's major true strain state varied between tension-tension in its central region (contact with the punch) shifting gradually to the plane strain state up to the region of contact with the die (where the predominant mechanism was becoming tension-compression).

Figure 8 summarizes the ε_1 distribution obtained with the three different punch geometries numerically studied. This graphic shows that with the cylindrical punch (P1), the maximum ε_1 point was moved toward the die's radius. By other hand, with the hemispherical punches (P3) and extra deep ellipse (P5), the ε_1 peak points remained closer to the punch pole.

4 Conclusion

The results described herein confirm that the material tended to suffer a greater stress concentration at the tool's smallest radius (congruence radius—R1), as indicated by the major true strain distribution profile measured from the die radius to the punch pole. The maximum ε_1 were found to occur close to the die radius when using the cylindrical and shallow ellipse punches (whose external congruence radius was smaller than the punch head radius) and close to the punch pole when using more pointed tools (deep and extra deep ellipse shaped punches).

From the comparison between the experimental and simulated data, it can be concluded that the ε_1 analysis via Finite Element Method, using ANSYS/LS_Dyna software, reproduces the experimental results satisfactorily.

The greatest dispersions between the simulated and experimental results occurred in the cases involving the cylindrical punch. The graphs displacements on the right or left in relation to the points of maximum ε_1 obtained should also not be considered as very relevant, i.e., the grid refinement causes the nodal distance to vary along the path selected for the reading data, and this variation was not taken into account when plotting the graphs.

We can, therefore, conclude that the ε_1 measurement along the test specimen (creating a profile) represents a useful tool for evaluating the critical punch action region upon the sheet. The ε_1 profile should be well adjusted for the desired tension-tension, tension-compression, and/or plane strain distribution preferentially during the tryout of stamping tools in order to obtain a more homogeneous stress/strain distribution. Qualitatively, it can be stated that the shape of the simulated and experimental curves are fairly similar to each other, and the numerical experimentation could be a successful way for reducing the costly try-and-error procedures.

Acknowledgments The authors are indebted to the ESSS Company and to Mr. Nicolau Botelho for the temporary supply of ANSYS/LS_Dyna software. We would like, also, to thank CAPES (Brazil) for granting a masters scholarship.

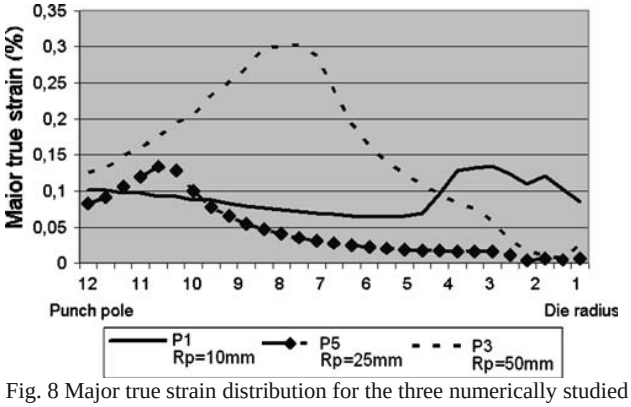

Fig. 8 Major true strain distribution for the three numerically studied punch geometries (P1, P3, and P5)—200×200-mm test specimens

References

1. Hongzhi D, Zhongqin L (2000) Investigation of sheet metal forming by numerical simulation and experiment. J Mater Process Technol, Shanghai 103:404–410
2. Makinouchi A (1996) Sheet metal forming simulation in industry. J Mater Process Technol 60:19–26
3. Fallbohmer P, Altan T, Tonshoff H-K, Nakagawa T (1996) Survey of the die and mold manufacturing industry. J Mater Process Technol 59:158–168
4. Hongzhi D, Teck CB, Jiang R, Zhongqin L (2002) Study on geometry modeling in the dynamic stamping simulation of a die. J Mater Process Technol 127:261–265
5. Buchar Z (1996) Circle grid analysis applied to the production problems of the car body panel. J Mater Process Technol 60:205–208
6. Koop R (1996) Some current development trends in metal forming technologies. J Mater Process Technol 60:1–9
7. Xu Y (2007) Formability analysis: finding the deformation zone, magazine metal forming, August, pp 36–39
8. Firat M (2007) Computer-aided analysis and design of the sheet metal forming processes: part I—the finite element modeling concepts. Mater Des 28(4):1298–1303
9. Yao H, Cao J (2002) Prediction of forming limit curves using an anisotropic yield function with prestrain-induced backstress. Int J Plast 18:1013–1038
10. Gronostajski J, Matuszak A, Niechajowicz A, Zimniak Z (2004) The system for sheet metal forming design of complex parts. J Mater Process Technol 157–158:502–507
11. Chemin Filho RA, Marcondes PVP (2008) True strain distribution profile on sheet metal using different punch geometries. Journal of the Brazilian Society of Mechanical Sciences and Engineering 30 (1):1–6
12. Mamalis AG, Manolakos DE, Baldoukas AK (1997) Simulation of sheet metal forming using explicit finite element techniques: effect of material and forming characteristics part 2 deep-drawing of square cups. J Mater Process Technol 72:110–116
13. Thamburaja P, Ekambaram R (2007) Coupled thermo-mechanical modelling of bulk-metallic glasses: theory, finite-element simulations and experimental verification. J Mech Phys Solids 55 (6):1236–1273
14. Hallquist JO (1998) LS-DYNA3D theoretical manual. Livermore Software Technology Corporation, Livermore
15. Barlat F, Lian J (1989) Plastic behavior and stretchability of sheet metals. Part1: a yield function for orthotropic sheets under plane stress conditions. Int J Plast 5:51–66
16. Ferziger JH, Peric M (2001) Computational methods for fluid dynamics, 3rd edn. Springer, Berlin
17. Oberkampf WL, Trucano TG, Hirsch C (2004) Verification, validation and predictive capability in computational engineering and physics. Appl Mech Rev, ASME 57:345–384